Application of a Deep Learning algorithm to Compton imaging of radioactive point sources with a single planar CdTe pixelated detector

G. Daniel [a, *], Y. Gutierrez [b], O. Limousin [b]

[a] Université Paris-Saclay, CEA, Service de Thermo-hydraulique et de Mécanique des Fluides, 91191, Gif-sur-Yvette, France
[b] AIM, CEA, CNRS, Université Paris-Saclay, Université Paris Diderot, Sorbonne Paris Cité, F-91191, Gif-sur-Yvette, France

ARTICLE INFO

ABSTRACT

Compton imaging is the main method for locating radioactive hot spots emitting high-energy gamma-ray photons. In particular, this imaging method is crucial when the photon energy is too high for coded-mask aperture imaging methods to be effective or when a large field of view is required. Reconstruction of the photon source requires advanced Compton event processing algorithms to determine the exact position of the source. In this study, we introduce a novel method based on a Deep Learning algorithm with a Convolutional Neural Network (CNN) to perform Compton imaging. This algorithm is trained on simulated data and tested on real data acquired with Caliste, a single planar CdTe pixelated detector. We show that performance in terms of source location accuracy is equivalent to state-of-the-art algorithms, while computation time is significantly reduced and sensitivity is improved by a factor of ~5 in the Caliste configuration.

© 2021 Korean Nuclear Society, Published by Elsevier Korea LLC. This is an open access article under the CC BY-NC-ND license (http://creativecommons.org/licenses/by-nc-nd/4.0/).

1. Introduction

Localization of radioactive hotspots is a crucial problematic in the frame of nuclear safety, for radiological scene monitoring, in the field of Decommissioning and Dismantling applications [1] or for nuclear medicine applications [2] and space science [3]. Gamma cameras constitute the principal solution to address this issue. They rely on the detection of high-energy gamma-ray photons, ranging from few keV up to ~2 MeV, associated to an image reconstruction method. Coded mask aperture is the main technique for gamma-ray photons with a sufficiently low energy to interact into the mask. Typically, 1-mm thick tungsten masks can be used for photons with energy up to 250 keV.

When the energy of the photons is getting higher, coded mask aperture imaging is no longer efficient. In fact, thicker masks degrade the image reconstruction properties and field of view due to the vignetting effect. Compton imaging is therefore a relevant method to perform radioactive hotspot localization of sources emitting high-energy photons. Moreover, above 250 keV, Compton scattering starts to be the dominant interaction process in CdTe.

In the following, we will use ^{137}Cs radioactive sources with an emission line at 662 keV to evaluate the response of our Compton reconstruction algorithm. This radioelement is used as a marker in nuclear safety applications and is often considered as a reference to evaluate high-energy imaging spectrometers' performances.

Compton imaging relies on the use of Compton scattering that corresponds to a partial deposition of the energy of the impinging photon, which is scattered with the rest of the energy.

If we denote E_0, the initial energy of the incident photon, E_1, the energy of the scattered photon, E_2, the energy deposited by the interaction and θ the scattering angle, the conservation of the total momentum of the system gives the Compton kinematics [4] in Equation (1):

$$\cos(\theta) = 1 - m_e c^2 \frac{E_1}{E_2 E_0} \tag{1}$$

$m_e c^2 = 511$ keV is the mass energy of electrons.

Equation (1) is valid only if the interacting electron in the material is at rest, which is not true in practice and this is the origin of the phenomenon known as Doppler broadening [5].

A system measuring the scattering direction and the energy deposition is able to provide the angular direction of the incident photon thanks to Compton kinematics. Since Equation (1) only gives the scattering angle, we can only derive a cone of the possible directions of origin of the photon. One source can then be localized

G. Daniel, Y. Gutierrez and O. Limousin

using several cones from a multitude of independent recorded photons.

Such systems, known as Compton cameras, have been extensively developed over the past decade. Focusing on semiconductor-based Compton cameras, some systems rely on the use of one or more detection layers with a low atomic number material, such as Si, as scattering layers followed by one or more absorbing layers with high atomic number material, such as CdTe [6,7]. On the other hand, some systems use 3D-position sensitive detectors with thick CdZnTe crystals [8]. In our setup, we use a single planar pixelated CdTe configuration, which is not advantageous a priori to perform Compton imaging compared to the aforementioned configurations. In any case, the recorded signals are complex and the direct projection of the cones, namely Simple BackProjection (SBP), may not provide sufficiently accurate positions. Therefore, more advanced algorithms must be further developed for Compton imaging. For instance, among the most advanced algorithms in the literature, we find iterative algorithms based on the Maximum Likelihood Expectation Maximization method, such as List-Mode (LM) MLEM [9]. We can also cite a stochastic algorithm based on Monte-Carlo Markov Chain, called Stochastic Origin Ensemble (SOE) [10] and one of its declinations, which considers uncertainties on interaction position and energy deposition, known as SOE with Resolution Recovery (SOE-RR) [11].

In this study, we present a novel method based on Deep Learning methods, especially on a Convolutional Neural Network (CNN). These methods have shown interesting performances in signal processing in the field of image recognition and are used in gamma-ray imaging for coded mask aperture systems [12–14]. To the best of our knowledge, these methods have never been applied to Compton imaging so far.

In this paper, we use the detection system Caliste-HD [15], a CdTe single planar pixelated detector with high energy resolution, to test our algorithm on real data acquisitions and for comparison with state-of-the-art methods applied to the same data sets.

The paper is structured as follows:

Section II briefly presents our detection system Caliste-HD and state-of-the-art Compton reconstruction algorithms. Section III focuses on the training method of our CNN, based on simulated data. Finally, we report our results on real test data in section IV and the comparison with other algorithms.

2. Compton imaging with Caliste-HD

2.1. Caliste-HD: A CdTe pixelated detector for gamma-ray photons

Caliste-HD [15] is a CdTe detector, equipped with a 1-mm thick crystal, with 16×16 pixels, 625 μm pixel-pitch. The total sensitive area is 1 cm^2 and each individual pixel is an independent spectrometer. The CdTe detector is associated to a dedicated ultra-low noise readout electronics, the IDeF-X HD ASICs [16,17].

The main advantage of Caliste-HD is its spectrometric

capabilities, which reaches a resolution of 670 eV FWHM (Full Width at Half Maximum) at 60 keV and 4.7 keV FWHM at 662 keV. Energy resolution is an important parameter for Compton imaging in order to apply the Compton kinematics formula. Each pixel has an individual dynamic range, which extends from 2 keV to 1 MeV. Table 1 summarizes the main characteristics of Caliste-HD.

These performances are reached at an operating temperature of $-10\ °C$ obtained by means of Peltier coolers. Therefore, the detection system is embedded in a portable device, the gamma-camera prototype WIX-HD, with a mass of 1 kg.

Under illumination, the WIX-HD camera records single and multi-events triggering its readout electronics. Hit channels, time and amplitudes feed an event list. According to each calibrated pixel parameters determined in advance, an energy calibrated event list is generated and used in the following.

2.2. Event selection in Caliste-HD for Compton imaging

A priori, the single planar configuration of Caliste-HD is not advantageous to perform Compton imaging. This detector was originally designed for applications in spectrometry or for Coded Mask Aperture imaging. However, we have demonstrated in [18] that this flaw is partially compensated by Caliste-HD's properties, especially its energy resolution and its fine-pitch. It indeed allows us to select carefully the relevant Compton events to reduce the background noise caused by irrelevant events.

Our pre-processing for Compton events selection is detailed in [18]. It consists of three steps. First, we select multiple events that are recorded in different pixels in time coincidence (corresponding to a unique trigger). Compton events are indeed composed of at least two simultaneous interactions in the detector, so that we can determine the scattering direction.

We defined an interaction as a single event, i.e. a single pixel hit, or a cluster of 2−4 adjacent pixels to take into account possible charge sharing and fluorescence escape. The interaction position will be defined as the energy-weighted barycentre of the hit positions. A relevant Compton event is a pair of interactions recorded in the same time period and separated by at least one untriggered pixel as represented in Fig. 1.

Finally, we perform a spectral selection, by assuming that we preliminarily know the radioisotope to localize, by means of an automatic identification algorithm for instance such as the one described in reference [19]. This selection consists of keeping events whose total energy deposited is close to an emission line of the identified radioisotope. In the present paper, we apply this selection to a ^{137}Cs source, with an energy window between 647 keV and 670 keV surrounding the emission line at 662 keV. Therefore, we only keep for processing events that Compton scattered and stopped with photoelectric absorption within the detector. Typically, after this selection, only 1 to 2 events per thousand are selected as Compton events.

2.3. Coordinates reference system

In the following parts, the reconstructed image will be represented in terms of longitude and latitude, following the spherical coordinate system represented in Fig. 2. The image represents a semi-sphere with both longitude and latitude between $-90°$ and $90°$. The discretization we use is $4°$ in longitude and latitude. Therefore, the localization accuracy is limited to the size of the discretization steps. Other configurations can be considered, especially a regular discretization of the sphere, but this is not in the scope of the present study.

Table 1
Characteristics of Caliste-HD.

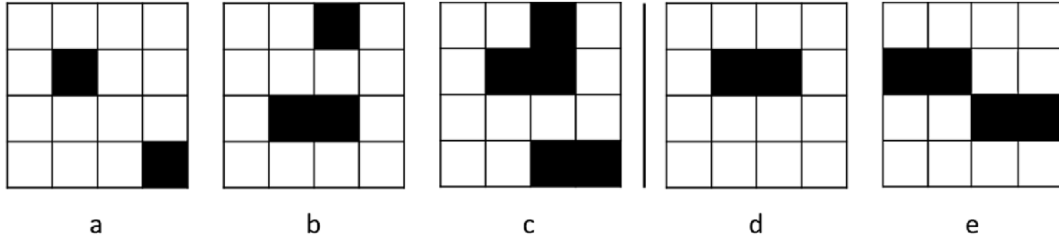| Parameter	CALISTE-HD
Number of pixels	256 (16×16)
Pixel Pitch	625 μm
Crystal thickness	1 mm
Dimension without CdTe	$10 \times 10 \times 16.5$ mm^3
Power Consumption	200 mW
Energy Range per pixel	2−1000 keV
FWHM at 60 keV	670 eV
FWHM at 662 keV	4.7 keV

G. Daniel, Y. Gutierrez and O. Limousin

Fig. 1. Several event configurations − Example of valid patterns used for Compton reconstruction are a: Two pixels separated, b: One single pixel and one cluster and c: Two clusters separated. Examples of rejected patterns are d: One cluster and e: Two unseparated clusters.
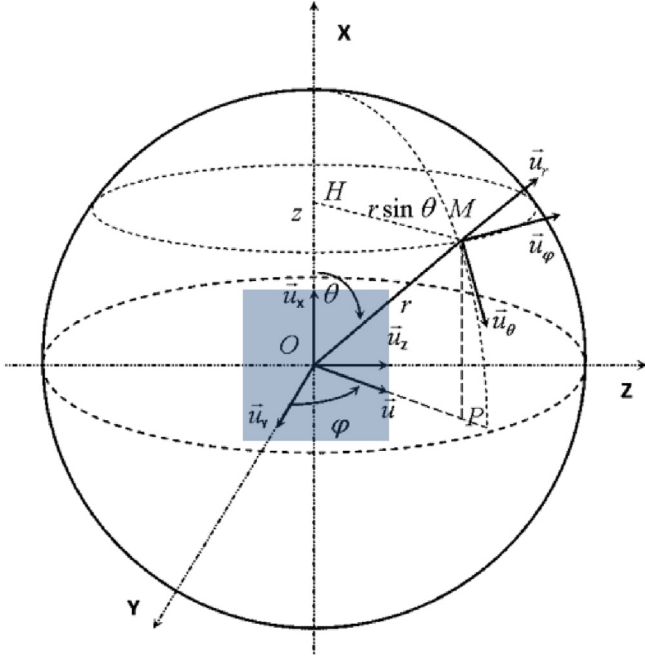

Fig. 2. Spherical coordinates system - The square represents the detector crystal.

2.4. Performance and limitations with SOE-RR, a state-of-the-art algorithm

SOE-RR is an iterative algorithm relying on the concept of Monte-Carlo Markov Chains (MCMC). It first attributes a random position j^0 on the Compton cone defined by each event i. For each iteration n, it draws another random position j^n and accepts or rejects the new position following a transition probability $p(j^{n-1} \rightarrow j^n)$. The latter is computed in order to favour positions j which concentrate the highest densities of events.

The Resolution Recovery version of SOE allows including physical considerations, especially uncertainties due to the detection system. It consists of adding randomness in the axis (according to the spatial resolution of the detector) and the angle (according to the spectral resolution of the detector) of the Compton cones.

By applying the SOE-RR algorithm [11,18] on real data acquisitions, we have previously achieved an angular resolution of 7.9° for a single point source and we were able to separate two point sources placed 10° apart, in a Field of View of 180°.

On the other hand, the planar configuration of our detector limits the sensitivity, here defined as the lowest achievable number of cones required to locate a point source. More than 2000 Compton cones are indeed required to perform the reconstruction with SOE-RR.

In Sections III and IV, we will demonstrate the contribution of the Deep Learning approach to the sensitivity, that surpasses SOE-RR.

Finally, we mention that LM-MLEM (List-Mode Maximum Likelihood Expectation Maximization) is another classical algorithm applied to Compton imaging. However, the application of this method leads to bad performances with our system, because of the uncertainties due to the geometrical configuration of our single planar 2D detector.

3. Convolutional Neural Network conception and training applied to Compton imaging

3.1. Simulated data set generation

It is necessary to train the network with as many positions as we want to recognize. Since we cannot possibly collect real data continuously for all the positions in the sky, we use Monte-Carlo simulations to create a training data set. We simulated the sources at 2025 separate positions between longitudes and latitudes −90° and 90° with a discretization step of 4°, in front of the detector. Each simulation contains about 140 000 Compton events from a single ^{137}Cs source located at a distance of 10 m from the virtual detector. We simulate only the 662 keV emission line.

The network does not operate directly on the event distributions given by the simulations. Only the relevant events are selected by the selection method as described in paragraph II.B. An image is constructed by application of the Simple BackProjection algorithm on those events, which then forms the input of the neural network. To recreate the constraints of real-world measurements, some information from the simulations is considered unknown. The interacting position of an event is rounded to the center of the pixel in which the event occurred, on the surface of the detector. The order of interaction is also considered unknown, and the photo-electric absorption of the scattered photon is systematically chosen to be the event with the smallest energy.

To account for the energy resolution of a real detector, the energies are drawn randomly in a Gaussian with a standard deviation of 6 keV around the exact values given by the simulation. This process may cause two cases that we systematically reject in the simulation:

- the recorded energy deposited by Compton scattering is higher than the Compton edge (i.e. 478 keV for the 662 keV emission line);
- the recorded energy deposited by photoelectric absorption is lower than the energy of a backscattered photon at 180° (i.e. 184 keV for the 662 keV emission line).

After the selection, the number of relevant events, and thus the number of projected cones, is reduced to around 10 000. The simulations also contain for each event the probability p_{Compton} that the photon would create a Compton event, i.e. a Compton
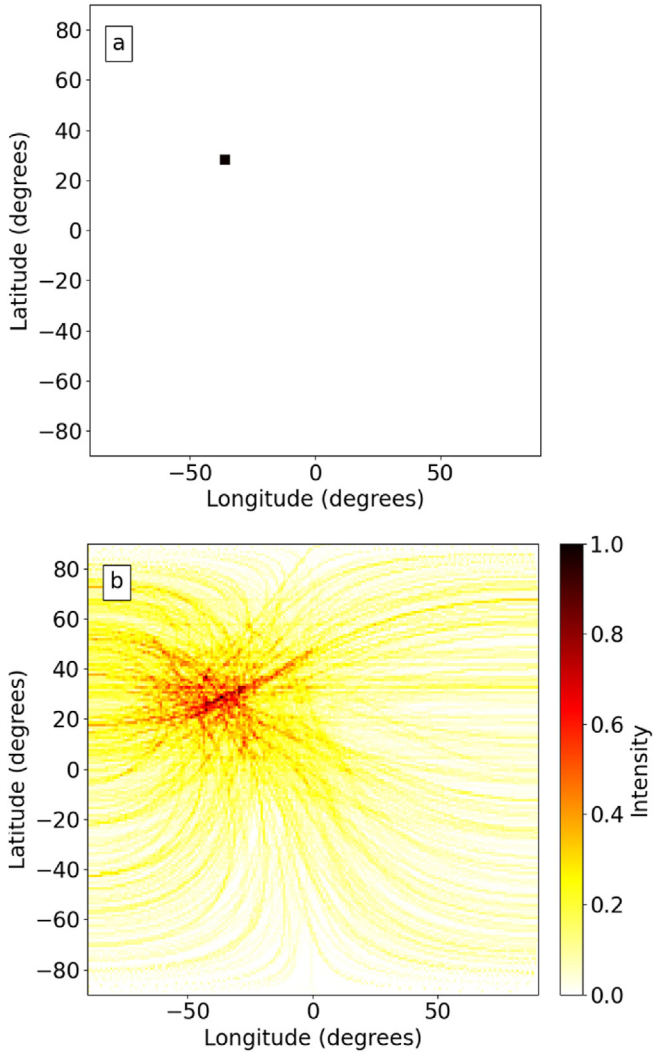
G. Daniel, Y. Gutierrez and O. Limousin

Fig. 3. a: Example of the position of a simulated source, it is the expected output of the neural network. b: Corresponding SBP.

interaction followed by a photoelectric absorption of the scattered photon.

The pixels of the back-projected image, which correspond to solid angles of size 2° by 2° in the field of view, are then normalized by their maximum to contain values between 0 and 1. This 90×90-pixel, 1-channel image is then passed to the network as input for training, along with a label containing the position of the source, corresponding to the desired output of the network for this particular input.

The output of the neural network is a vector with 2025 elements corresponding to the 2025 simulated positions with a discretization of 4° by 4°, with a 1 for the label corresponding to the simulated position and 0 for the other positions. This vector is then represented as a 45×45 image, from $-90°$ to $90°$ in both longitude and latitude with the discretization step of 4°.

Fig. 3 shows an example of a simulated position on a 45x45 image, which represents a training output for the neural network, and the corresponding SBP, which is the corresponding input for the network.

3.2. Architecture of the CNN

For the conception of the CNN, we use an architecture adapted from the AlexNet architecture [20], which consists of several convolutional layers followed by fully-connected layers. This architecture was initially designed for image processing, especially image recognition tasks, and seems a priori relevant for our problematic.

We have adapted the architecture to our data format, so that the inputs are 90×90, 1-channel images and the output is a 2025 elements vector. The final architecture is given in Fig. 4.

3.3. Training of the CNN with a dynamic database

We use a dynamic database, also called "online learning", to train our CNN. To build one example, we randomly draw a position and then we pick up a random number of cones, between 30 and 3000, in the simulation described in paragraph III.A to create the corresponding backprojection. The probability to pick up one specific cone is proportional to the factor $p_{Compton}$ associated to this cone in the simulation. We create this way a sample of 1000 examples. Then we train our CNN with one epoch on these 1000 examples and we iterate this process by generating 1000 new examples and doing one training step. This process is done 2000 times, which means that we show 2 million different examples to the CNN.

For the training, we use the categorical cross-entropy loss function, given by Equation (2):

$$L(\widehat{Y}, Y) = \sum_{\text{position } i} y_i \log(\widehat{y}_i) \qquad (2)$$

where $\widehat{Y} = (\widehat{y}_i)_i$ is the vector containing the predictions of the neural network for each position i and $Y = (y_i)_i$ is the vector encoding the real position of the source: $y_i = 1$ if i is the position of the source, else $y_i = 0$.

The optimization algorithm for the training is Adam (Adaptive Moment Estimation) [21] with a learning rate of 10^{-4}, $\beta_1 = 0.9$, $\beta_2 = 0.999$ (moment-related parameters in the Adam algorithm) and $\varepsilon = 10^{-8}$ (constant of the Adam algorithm for numerical stability). We use the Pytorch library [22] and GPU parallelization on an NVIDIA GeForce RTX 2080 Ti 11 GB. The training time for 2000 iterations is about one week.
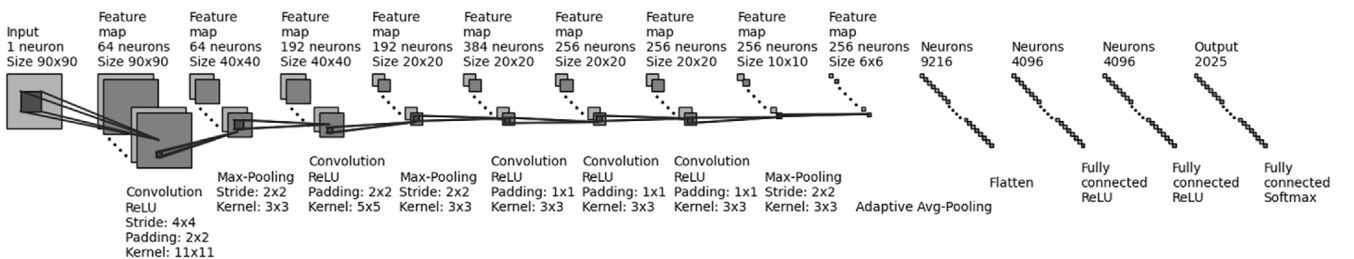

Fig. 4. Architecture of the CNN, adapted from AlexNet.

G. Daniel, Y. Gutierrez and O. Limousin

Table 2
Characteristics of the measurements.

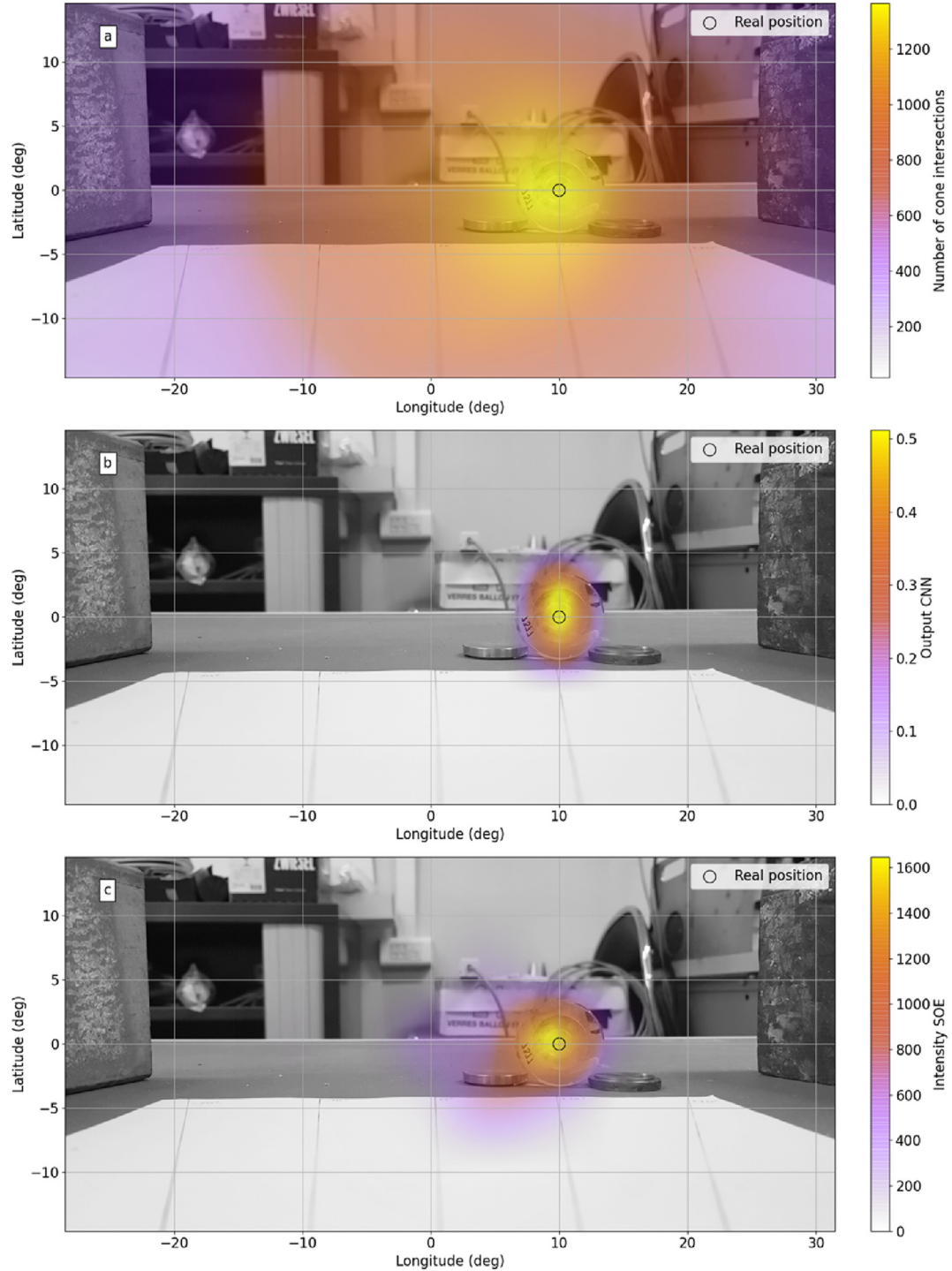| Position of the source (longitude and latitude)	Source activity	Measurement time	Total number of counts	Number of selected Compton events
(0°,0°)	1.7 MBq	35.6 h	3190418	4855
(10°,0°)	1.7 MBq	57.7 h	5423829	8065
(30°,0°)	1.7 MBq	83.8 h	6993265	12222
(35°,0°)	1.7 MBq	19.5 h	1672290	3014
(40°,0°)	1.7 MBq	76.8 h	4791771	11581
(-22°,33°)	3.6 MBq	61.1 h	8213658	17978

Fig. 5. Results of the algorithms applied to the (10°,0°) position measurement. a: Simple BackProjection. b: CNN. c: SOE-RR. An interpolation (spline16 with the *matplotlib* library) has been applied to the Compton reconstruction for representation purposes.
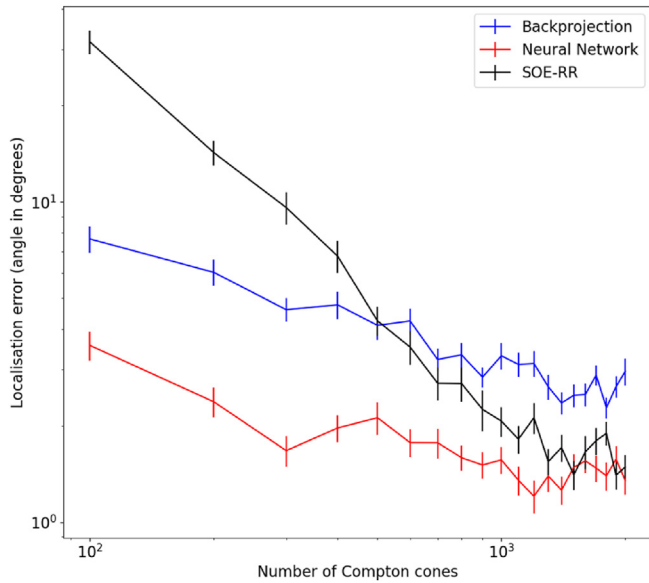
G. Daniel, Y. Gutierrez and O. Limousin

Fig. 6. Localization error of the algorithms vs the number of Compton events used in the reconstruction. The scale is log-log.

4. Results and discussion

Our CNN based reconstruction algorithm has been optimized by means of simulations. In this section, we apply the network to real data and compare the results with SOE-RR on the exact same data set (event lists).

4.1. Experimental setup

We have made six acquisitions to build a test set with real data. Each acquisition consists of a measurement with Caliste-HD from a ^{137}Cs source, at 30 cm from the detector. The corresponding dose rate at detector level is ~1.4 μSv/h for the 1.7 MBq source and ~2.9 μSv/h for the 3.6 MBq source.

Table 2 gives the positions of the source and the characteristics of each measurement. The precision of the positioning of the source is given with about 3° uncertainties. The total number of counts takes into account of the multiplicity of each hit: several triggers occurring at the same time in different pixels are counted as one hit.

4.2. Application of CNN and SOE-RR algorithms to process Compton imaging

We show in Fig. 5 one reconstruction example for the measurement at the position (0°,10°). We apply the SOE-RR and CNN algorithms to the full measurement, and we also show the SBP image, which is the input of the CNN. The gamma image is superimposed on an optical image taken by an optical camera at the detector position. We highlight that the Field of View of the gamma image is 180° and we represent only a partial area of this Field of

View, restricted to the optical image.

SOE-RR is applied with 20 000 iterations. This parameter can be optimized, it is chosen here as it insures the convergence of the algorithms. Each algorithm is able to reconstruct the correct position of the source.

4.3. Performance assessment and algorithm benchmark

To evaluate the localization performance of the algorithms, we build a test dataset with the six measurements described in Table 2. We consider n Compton events, where n varies from 100 to 2000, with a step of 100. For each number n of Compton events, we build 100 examples by randomly drawing n Compton events in the measurements. For each example, we apply the algorithms (SBP, CNN, SOE-RR) and we compute the angular difference between the true position and the position with a maximum intensity given by the algorithms. The real position is known with 3° uncertainty, which is taken into account in the error computation.

Fig. 6 shows the average of the localization error computed for 100 examples for each number of Compton events n used for the reconstruction. The error bar is computed as the standard deviation on the 100 results for each n. SOE-RR is applied with 20 000 iterations.

Our CNN shows a better performance compared to all of the other algorithms when the number of Compton events is lower than 1100. After 1200 events, SOE-RR and CNN have similar performances. CNN reaches a localization error lower than 3° with only 200 cones while SOE-RR reaches this performance with 900 cones, which shows that CNN has a much higher sensitivity, about 5 times better than SOE-RR.

Moreover, SOE-RR has a worse performance than the other algorithms if the number of Compton cones is too low (lower than 400 cones). If the number of cones is too low, SOE-RR does not converge and is more likely to assign a random position to the source.

We compare in Table 3 the computation time of each algorithms for 2000 Compton events. Each algorithm has been individually optimized in terms of computation time.

In Table 3, the computation time of our CNN includes both the computation time of the SBP, which is necessary to produce the input image for the CNN, and the computation of the CNN itself. The computation time of the CNN alone is about 30 ms, which is negligible compared to the SBP. Moreover, the computation time does not depend on the number of Compton events used in the reconstruction. Consequently, the computation time of the whole CNN calculation relies only on the computation time of the SBP, which is proportional to the number of Compton events to be processed.

SOE-RR takes much longer to process. Its computation time depends on both the number of iterations and the number of processed Compton events.

5. Conclusion and outlooks

We have developed a new method based on Convolutional Neural Networks to perform Compton image reconstruction. Our CNN has been trained on simulated data and tested on real data measurements with a ^{137}Cs source. Compared to SOE-RR, another classical state-of-the-art algorithm, we evaluated that our CNN has better localization performances in terms of localization error and a sensitivity ~5 times better than the SOE-RR algorithm. In addition, the computation time of our CNN is equivalent to the SBP, which is the fastest existing Compton reconstruction algorithm so far.

The development and the tests of the CNN have been conducted in the case of the localization of a single point source. The presented

Table 3
Computation time for 2000 Compton events.

Algorithm	Time (s)
SBP	1.80±0.01
CNN	1.83±0.02
SOE-RR (20 000 iterations)	56.2±1.5

results provide a rationale to carry out studies in more complex scenes, with several point sources or extended sources and several radioelements. The learning method must be adapted to the application. Other neural network architectures that are a priori relevant for this application should also be considered, the most promising ones being convolutional autoencoders, which consist in convolution/deconvolution operations in order to reconstruct a filtered image. Finally, modifications of the detector system will be studied to perform 3D positioning of the interactions in the detector crystal, in order to reduce uncertainties and further improve the sensitivity.

Declaration of competing interest

The authors declare that they have no known competing financial interests or personal relationships that could have appeared to influence the work reported in this paper.

Acknowledgement

References

[1] Y.-s. Kim, J.H. Kim, H.S. Lee, H.R. Lee, J.H. Park, J.H. Park, H. Seo, C. Lee, S.H. Park, C.H. Kim, Development of Compton imaging system for nuclear material monitoring at pyroprocessing test-bed facility, J. Nucl. Sci. Technol. 53 (12) (2016) 2040−2048.

[2] A. Koide, J. Kataoka, T. Masuda, S. Mochizuki, T. Taya, K. Sueoka, L. Tagawa, K. Fujieda, T. Maruhashi, T. Kurihara, T. Inaniwa, Precision imaging of 4.4 MeV gamma rays using a 3-D position sensitive Compton camera, Sci. Rep. 8 (2018). Article number: 8116.

[3] T. Tanaka, R. Blandford, K. Doutsu, T. Endo, T. Enoto, Y. Fukazawa, K. Fukami, T. Fukuyama, Y. Hanabata, J. Harayama, K. Hayashi, K. Hiragi, S. Ishikawa, J. Kataoka, J. Katsuta, T. Kitaguchi, M. Kokubun, M. Koseki, T. Kozu, G. Madejski, K. Makishima, K. Matsuoka, T. Miura, T. Mizuno, S. Nakahira, K. Nakajima, K. Nakazawa, S. Nishino, H. Nishioka, H. Noda, H. Odaka, S. Saito, S. Sasaki, R. Sato, S. Sugimoto, H. Tajima, T. Takahashi, M. Tashiro, Y. Terada, S. Torii, Y. Uchiyama, Y. Umeki, S. Watanabe, Y. Yaji, S. Yamada, K. Yamaoka, M. Yoshino, T. Yuasa, The Soft Gamma-Ray Detector for the ASTRO-H Mission, IEEE Nuclear Science Symposium Conference Record (NSS/MIC), 2009, pp. 2140−2144.

[4] W. Leo, Techniques for Nuclear and Particle Physics Experiments: A How-To Approach, Springer-Verlag, 1993.

[5] E. Ordonez, A. Bolozdynya, W. Chang, Doppler Broadening of Energy Spectra in Compton Cameras, 1997, 2, IEEE Nuclear Science Symposium Conference Record, Albuquerque, NM, USA, 1997, pp. 1361−1365.

[6] S. Takeda, Y. Ichinohe, K. Hagino, H. Odaka, T. Yuasa, S.-n. Ishikawa, T. Fukuyama, S. Saito, T. Sato, G. Sato, S. Watanabe, M. Kokubun, T. Takahashi, Applications and imaging techniques of a Si/CdTe Compton gamma-ray camera, TIPP 2011 - technology and instrumentation in particle physics 2011, Phys. Procedia 37 (2012) 859−866, 2012.

[7] G. Llosa, M. Trovato, J. Barrio, A. Etxebeste, E. Muñoz, C. Lacasta, J.F. Oliver, M. Rafecas, C. Solaz, P. Solevi, First images of a three-layer Compton telescope prototype for treatment monitoring in hadron therapy, Front. Oncol. 6 (14) (2016).

[8] C. Lehner, Z. He, F. Zhang, 4Pi Compton imaging using a 3-D position-sensitive CdZnTe detector via weighted list-mode maximum likelihood, IEEE Trans. Nucl. Sci. 51 (4) (2004).

[9] L. Parra, H. Barrett, List-mode likelihood: EM algorithm and image quality estimation demonstrated on 2-D PET, IEEE Trans. Med. Imag. 17 (2) (1998).

[10] A. Andreyev, A. Sitek, A. Celler, Fast image reconstruction for Compton camera using stochastic origin ensemble approach, Nucl. Med. Phys. 38 (1) (2010) 429−438.

[11] A. Andreyev, A. Celler, I. Ozsahin, A. Sitek, Resolution recovery for Compton camera using origin ensemble algorithm, Med. Phys. 43 (8) (2016) 4866.

[12] R. Zhang, P. Gong, X. Tang, P. Wang, C. Zhou, X. Zhu, L. Gao, D. Liang, Z. Wang, Reconstruction method for gamma-ray coded-aperture imaging based on convolutional neural network, Nucl. Instrum. Methods Phys. Res. A 934 (2019) 41−51.

[13] R. Zhang, X. Tang, P. Gong, P. Wang, C. Zhou, X. Zhu, D. Liang, Z. Wang, Low-noise Reconstruction Method for Coded-Aperture Gamma Camera Based on Multi-Layer Perceptron, Nuclear Engineering and Technology, 2020.

[14] G. Daniel, O. Limousin, Extended Sources Reconstructions by Means of Coded Mask Aperture Systems and Deep Learning Algorithm, Submitted to NIM-A, 2021.

[15] S. Dubos, O. Limousin, C. Blondel, R. Chipaux, Y. Dolgorouky, O. Gevin, Y. Ménesguen, A. Meuris, T. Orduna, T. Tourette, A. Sauvageon, Low energy characterization of Caliste HD, a fine pitch CdTe-based imaging spectrometer, IEEE Trans. Nucl. Sci. 60 (No. 5) (2013).

[16] A. Michalowska, O. Gevin, O. Lemaire, F. Lugiez, P. Baron, H. Grabas, F. Pinsard, O. Limousin, E. Delagnes, IDeF-X HD : a low power multi-gain CMOS ASIC for the readout of Cd(Zn)Te detectors, in: IEEE Nuclear Science Symposuim and Medical Imaging Conference, 2010. NSS/MIC p. 1556-1559 5874037.

[17] O. Gevin, F. Lugiez, A. Michalowska, A. Meuris, O. Limousin, E. Delagnes, O. Lemaire, F. Pinsard, IDeF-X HD: a CMOS ASIC for the Readout of Cd(Zn)Te Detectors for Space-Borne Applications, 2020 arXiv:2102.01992.

[18] G. Daniel, O. Limousin, D. Maier, A. Meuris, F. Carrel, Compton imaging reconstruction methods: a comparative performance study of direct back-projection, SOE, a new Bayesian algorithm and a new Compton inversion method applied to real data with Caliste, in: EPJ Web Conf, 225, ANIMMA, 2019, p. 2020.

[19] G. Daniel, F. Ceraudo, O. Limousin, D. Maier, A. Meuris, Automatic and real-time identification of radionuclides in gamma-ray spectra: a new method based on convolutional neural network trained with synthetic data set, IEEE Trans. Nucl. Sci. Proc.Animma. 67 (4) (2019) 644−653, 2020.

[20] A. Krizhevsky, I. Sutskever, G. Hinton, ImageNet classification with deep convolutional neural networks, Commun. ACM 60 (Issue 6) (2017).

[21] D. Kingma, J. Ba, Adam: a method for stochastic optimization, in: Conference Paper at the 3rd International Conference for Learning Representations, 2015. San Diego.

[22] A. Paszke, S. Gross, F. Massa, A. Lerer, J. Bradbury, G. Chanan, T. Killeen, Z. Lin, N. Gimelshein, L. Antiga, A. Desmaison, A. Kopf, E. Yang, Z. DeVito, M. Raison, A. Tejani, S. Chilamkurthy, B. Steiner, L. Fang, J. Bai, S. Chintala, PyTorch: an imperative style, high-performance deep learning library, Adv. Neural Inf. Process. Syst. 32 (2019) 8024−8035. NEURIPS2019.